JOURNAL OF VIROLOGY, Aug. 2010, p. 7543–7557 Vol. 84, No. 15
0022-538X/10/$12.00 doi:10.1128/JVI.00477-10

Phosphatidylinositol 3-Kinase-, Actin-, and Microtubule-Dependent Transport of Semliki Forest Virus Replication Complexes from the Plasma Membrane to Modified Lysosomes[▽]†

Pirjo Spuul,*§ Giuseppe Balistreri,§ Leevi Kääriäinen, and Tero Ahola

Institute of Biotechnology, University of Helsinki, Helsinki, Finland

Received 3 March 2010/Accepted 12 May 2010

Like other positive-strand RNA viruses, alphaviruses replicate their genomes in association with modified intracellular membranes. Alphavirus replication sites consist of numerous bulb-shaped membrane invaginations (spherules), which contain the double-stranded replication intermediates. Time course studies with Semliki Forest virus (SFV)-infected cells were combined with live-cell imaging and electron microscopy to reveal that the replication complex spherules of SFV undergo an unprecedented large-scale movement between cellular compartments. The spherules first accumulated at the plasma membrane and were then internalized using an endocytic process that required a functional actin-myosin network, as shown by blebbistatin treatment. Wortmannin and other inhibitors indicated that the internalization of spherules also required the activity of phosphatidylinositol 3-kinase. The spherules therefore represent an unusual type of endocytic cargo. After endocytosis, spherule-containing vesicles were highly dynamic and had a neutral pH. These primary carriers fused with acidic endosomes and moved long distances on microtubules, in a manner prevented by nocodazole. The result of the large-scale migration was the formation of a very stable compartment, where the spherules were accumulated on the outer surfaces of unusually large and static acidic vacuoles localized in the pericentriolar region. Our work highlights both fundamental similarities and important differences in the processes that lead to the modified membrane compartments in cells infected by distinct groups of positive-sense RNA viruses.

All positive-strand RNA viruses replicate their genomes in association with cellular membranes. The formation and activity of the membrane-bound replication complexes (RCs) can result in extensive alteration of membrane structures (11, 40, 48). Different viruses use different cytoplasmic membrane compartments as platforms for replication. Currently, there is only a limited understanding of how the virus-encoded and cellular proteins coordinate the formation of the replication-induced membrane structures. We address the mechanisms of membrane-bound replication with alphaviruses, particularly Semliki Forest virus (SFV). The alphaviruses comprise several human and animal pathogens, including the encephalitogenic alphaviruses (e.g., Western, Eastern, and Venezuelan equine encephalitis viruses) as well as the recently reemerging chikungunya virus, which belongs to the SFV clade of alphaviruses. During the past 5 years, chikungunya virus has caused more than 2 million infections and 500 deaths, and a new strain has spread throughout the areas surrounding the Indian Ocean (50). The alphaviruses use mosquitoes as intermediate hosts and transmission vectors, and at present no vaccines or antivirals are available to control these infections.

The cytoplasmic replication of alphaviruses depends on the four viral nonstructural (ns) proteins, nsP1 to nsP4, which are all essential and act as a membrane-bound replication complex. The nsPs are translated from the viral positive-sense RNA genome as one large polyprotein. Cleavages catalyzed by the nsP2 moiety result in the release of the individual proteins. A large fraction of the synthesized nsPs is involved in genome replication and associates with membranes, but a sizable fraction dissociates and is distributed in different cellular compartments: nsP1 binds to the inner surface of the plasma membrane (PM); nsP2 is translocated into the nucleus; nsP3 seems to form aggregates in the cytoplasm; and most of the extra nsP4, the core RNA polymerase, is degraded by the proteasome. While the major enzymatic functions of the individual nsPs have been elucidated (21), little is known of how they function together in the replication machinery.

As in other positive-strand RNA viruses, the RCs of alphaviruses are associated with altered intracellular membranes, which were first described in the late 1960s and early 1970s (13, 14, 18). In these early studies, it was shown that virus replication induces bulb-shaped membrane invaginations with a diameter of ~50 nm, which were called spherules. The spherules were found on the limiting membranes of large cytoplasmic vacuoles, which were named virus-induced *cyto**p**athic **v**acuoles of type **I*** (CPV-I). On rare occasions, the spherules were seen also at the PM. By electron microscopic (EM) autoradiography, it was also shown that the spherules both at the CPV-I and at the PM could be sites of RNA synthesis (18). Subsequently, Froshauer et al. (15) showed that CPV-I are positive for endosomal and lysosomal markers. Moreover, using EM, they showed that the inside of the spherule is connected to the cytoplasm by a pore from which electron-dense material

* Corresponding author. Mailing address: Institute of Biotechnology, P.O. Box 56, 00014 University of Helsinki, Finland. Phone: 358-9-19159398. Fax: 358-9-19159560. E-mail: pirjo.spuul@helsinki.fi.

† Supplemental material for this article may be found at http://jvi.asm.org/.

§ P.S. and G.B. contributed equally to this work.

▽ Published ahead of print on 19 May 2010.

(which the authors suggest to be the newly synthesized RNA) seems to diffuse into the cytoplasm.

During the past decade, our group has addressed the biogenesis of the CPV-I. We demonstrated that the formation of the spherules did not require structural proteins (44) and, more recently, that all four nsPs were associated with the spherules together with newly formed RNA (labeled by bromouridine), strongly suggesting that they were the actual units of RNA replication (RCs) (28). We also suggested as one possibility that the spherules could first arise at the PM; subsequent endocytosis of the spherules could account for the formation of the CPV-I (28, 44). Of the four nsPs, only nsP1 has affinity for membranes, and when expressed alone, it is specifically targeted to the inner surface of the PM (45). NsP1 is a monotopic membrane protein; its affinity for membranes is dictated by an amphipathic alpha helix, located in the central region of the protein (4, 31). NsP1 has a specific affinity for negatively charged phospholipids, which could potentially account for its prevalent localization to the PM, where such lipids are enriched. Later we showed that the membrane binding of nsP1 through the amphipathic helix is essential for alphavirus replication (56).

Several groups of positive-sense RNA viruses make spherules, which appear very similar to those made by the alphaviruses. However, for these virus groups, the spherules arise in different locations. For the well-characterized brome mosaic virus (BMV), a plant virus very distantly related to the alphaviruses, the spherules are seen in the endoplasmic reticulum (ER) adjacent to the nucleus (51). For the unrelated nodaviruses, the spherules are localized on mitochondrial surfaces (25). Recent models of the RCs of flaviviruses suggest that their replication complexes also resemble spherules (62). For the *Flaviviridae*, the RCs are found on the membranes of the secretory pathway.

The aim of this study was to clarify the role of different membranes in the formation and maturation of alphavirus RCs, and particularly to test our hypothesis that the RCs (spherules) are formed at the PM and are internalized thereafter. By using confocal microscopy, live-cell imaging, and novel electron microscopic techniques, we demonstrate that the RCs of SFV undergo an unprecedented, highly dynamic trafficking between different cellular compartments. They are first detected at the PM, which serves as the major platform for spherule formation. A specific endocytic event results in the transfer of spherules to the limiting membrane of small cytoplasmic vesicles. Using pharmacological inhibitors, we have been able to block the internalization process, and we found that the exit of spherules from the PM is dependent on the activity of phosphatidylinositol3- kinase (PI3K). Following the intracellular dynamics associated with spherules in live cells, we show the contribution of actin and microtubule-based transport, as well as that of fusion events with preexisting acidic organelles, providing the first complete model for the biogenesis of the large static CPV-I, where spherules are found at later stages of infection.

MATERIALS AND METHODS

Cell culture. BHK-21 cells (baby hamster kidney cells) were maintained in Dulbecco's modified Eagle's medium (DMEM) supplemented with 7.5% fetal bovine serum (FBS; Gibco-BRL, Grand Island, NY), 2% Bacto tryptose phosphate broth (Difco Laboratories, Detroit, MI), 2 mM L-glutamine, 100 U/ml penicillin, and 100 μg/ml streptomycin (Gibco). Primary mouse embryonic fibroblasts (MEFs), derived from 17-day-old embryos, and HeLa cells were cultured in DMEM supplemented with 10% FBS, 2 mM L-glutamine, 100 U/ml penicillin, and 100 μg/ml streptomycin.

Plasmid constructs. The pSFV-ZsG plasmid was designed to contain ZsGreen fluorescent protein fused with nsP3. The ZsGreen sequence was amplified by PCR from the pZsGreen plasmid (Clontech Laboratories, Inc., Mountain View, CA), and CTCGAG (XhoI site) was added to both ends of the sequence. The resulting PCR product was inserted into the XhoI sites of pSFV4 infectious cDNA and the pSFV1 replicon (33).

Antibodies and reagents. Rabbit polyclonal anti-nsP3 has been described previously (28). Mouse monoclonal antibody J2 against double-stranded RNA (dsRNA) was purchased from Scicons (Hungary). Mouse monoclonal antibodies against α-tubulin and γ-tubulin were obtained from Sigma-Aldrich, Inc. (St. Louis, MO) and GM130 antibody from BD Transduction Laboratories (San Jose, CA). Phalloidin-AF568 and LysoTracker Red DND-99 were purchased from Molecular Probes (Eugene, OR), as were the secondary antibodies with AF488 and AF568 fluorophores.

(−)-Blebbistatin, wortmannin, LY294002, and PI-103 were purchased from Sigma. Nocodazole for tubulin disruption was obtained from Calbiochem (Merck KGaA, Germany).

Viruses, growth curve experiments, and drug treatments. Wild-type (wt) SFV and SFV-ZsG were obtained from cloned cDNA as described previously (56). Sindbis virus (SIN) was similarly obtained from the cDNA clone pTOTO1101, a kind gift from Charles M. Rice. For growth curve determination, BHK-21 cells were infected with 10 PFU/cell for 1 h in infection medium (MEM plus 0.2% bovine serum albumin [BSA] plus 2 mM L-glutamine) and were then washed extensively. New medium was added, and 100-μl aliquots were withdrawn at the time points indicated in Fig. 3A. Virus titers were determined by a plaque assay (23). Virus growth curves in the presence of inhibitors were obtained by using SFV-ZsG. BHK-21 cells were infected at a multiplicity of infection (MOI) of 10 for 1 h and were then washed five times. New medium containing the respective drugs was added, and aliquots of 100 μl were withdrawn at the time points indicated in Fig. 7. Virus titers were obtained by infecting BHK-21 cells with dilutions of the collected samples and counting the number of nsP3-ZsG-positive cells by direct fluorescence at 4 h postinfection (p.i.). Western blotting was performed as described previously (30).

For live-cell imaging, virus replicon particles (VRPs) were used instead of infectious SFV-ZsG for safety reasons. The split-helper system was applied to package the SFV1 replicon RNA into the VRPs (52).

For drug treatments, BHK-21 cells were infected with 500 PFU/cell for 20 min in infection medium; then they were washed extensively, and fresh medium was added. Drugs were added at 20 min or 1 h 30 min p.i., depending on the experiment, and cells were fixed at 2 h or 4 h p.i., respectively. For microtubule disruption, nocodazole was added from the beginning of the infection. LY294002 washout was performed after 4 h of infection (a 2-h 30-min drug treatment), and samples were fixed at 8 h p.i.

Viral RNA synthesis. BHK-21 cells were infected with wt SFV at an MOI of 10 for 1 h. After five washes, new medium containing the respective drugs and 2 μg/ml of actinomycin D was added. Untreated or mock-infected samples served as controls. Duplicate dishes of each set were pulse-labeled at 4.5 h p.i. and 5.5 h p.i. with 25 μCi/dish of [^{3}H]uridine for 30 min in the presence of actinomycin D (2 μg/ml). Samples were washed twice with cold phosphate-buffered saline (PBS) and were lysed with 2% sodium dodecyl sulfate (SDS) in PBS at 65°C. Labeled RNAs were precipitated in 10% trichloroacetic acid (TCA) on ice for 1 h. Precipitates were collected on glass fiber filters (GF/C; Whatman) and washed twice with 5% TCA, and the incorporated [^{3}H]uridine was quantified by liquid scintillation (Optiphase Supermix; Perkin-Elmer) counting.

Indirect immunofluorescence. Cells were fixed at room temperature with 4% paraformaldehyde in phosphate-buffered saline for 15 min, quenched with 50 mM NH_4Cl, and permeabilized with 0.1% Triton X-100. The samples were incubated for 1 h at room temperature with primary antibodies, followed by washes and 1 h of incubation with appropriate secondary antibodies. Mowiol 4-88 (Calbiochem) containing 2.5% DABCO [1,4-diazabicyclo(2,2,2) octane; Sigma] was used for mounting the coverslips.

Microscopy. Fixed samples were analyzed with a Leica TCS SP5 upright confocal microscope using an HCX APO 63×/1.30 numerical aperture, corrected for 21°C glycerol objective. In addition, an Olympus AX-70 Provis microscope with a 20×/0.50 Ph1 air objective was used to take field pictures for quantification analysis. Pictures were collected by a Photometrics SenSys air-cooled charge-coupled device (CCD) camera using the AnalySIS program. The exposure was always set to 200 ms for dsRNA imaging.

For live-cell imaging, cells were grown in no. 0 glass-bottom culture dishes (MatTek, Ashland, MA), and MEM supplemented with 0.2% BSA, 2 mM L-glutamine, and 20 mM HEPES (pH 7.4) was used as an imaging medium. The Olympus IX71 TILL imaging system supplemented with a 37°C chamber and CO_2 was used to image the live cells with a UPlanSApo 60× 1.20 numerical aperture water objective. Images were acquired at the rate of 2 frames/s (2 Hz). A Leica TCS SP2 confocal microscope supplemented with a 37°C chamber and CO_2 was used to image the live cells with an HCX PL APO 63×/1.20 numerical aperture, corrected for a 0.17-mm cover slip, water objective. Live-cell recordings were done with bidirectional scanning at a speed of 800 Hz; image stacks were acquired at the rate of 0.5 or 1 frame/s (0.5 or 1 Hz) as specified in the figure legends. To visualize the acidic compartment of the cell, LysoTracker was added to the sample 20 min before imaging and was present during the recordings.

For correlative light-electron microscopy (CLEM), cells were grown in no. 2 glass-bottom P35G-2-14-C-Grid dishes (MatTek). After glutaraldehyde fixation, samples were analyzed with a Leica TCS SP2 confocal microscope using an HC PL APO 20×/00.7 CS air objective and an HCX PL APO 63×/1.2 water objective for larger magnifications. To visualize the grid, the microscope was set to reflection mode. For transmission electron microscopy (TEM), chemically fixed and osmium-stained cells were processed for flat embedding and ultrathin sectioning as described previously (46). A JEOL 1200 EX II transmission electron microscope operated at 80 kV was used for imaging. Scanning electron microscopy (SEM) was performed using a Zeiss DSM 962 microscope. Before imaging, cell monolayers (processed as for TEM) were covered with hexamethyldisilazane (Fluka) and were allowed to dry overnight at room temperature.

Image analysis. SFV phenotypes were defined based on quantitative determinations of the localization of RCs in time course experiments or in the presence of drugs by using ImageJ (National Institutes of Health, Bethesda, MD). In all cases, the borders of approximately 100 cells were drawn manually in each imaging field (in 4 to 5 fields per experiment), and the cells were visually classified into three phenotypic groups according to the localization of the RCs. The early stage corresponded to strong PM staining; the second (intermediate) stage was characterized by partial PM staining and small, scattered cytoplasmic puncta; the late stage was defined as showing little PM signal and larger puncta in the perinuclear area. The standard deviation (SD) was calculated for each sample group.

Live recordings from the Olympus TILL imaging system (see videos S1 and S2 in the supplemental material) were processed with TILLvisION (TILL Photonics GmbH) and were analyzed with Image-Pro Plus (Media Cybernetics, Inc.) and Bitplane Imaris (Bitplane Inc.).

Selected confocal stacks (see Fig. 2A, 3Ca and D, 5A, and 6A and B) were deconvoluted with AutoQuant AutoDeblur 3D Blind Deconvolution (AutoQuant Imaging, Inc.). Bitplane Imaris was used to make 3-dimensional (3D) reconstructions as maximum projections (see Fig. 3Ca and D, 4A, B, and E, 5A and B, and 6A and B), orthoslices (see Fig. 2A), and isosurface renderings (see Fig. 6A and B) and to process the live-cell imaging data from confocal microscopy (see videos S3 and S4 in the supplemental material). A Gaussian filter with a 0.13-μm filter width was applied to live recordings. Tracks and speed for the RC trafficking were calculated using the Imaris spot-tracking function (Fig. 4A and B, 5B, and 6C). Spherules were quantified manually after TEM and SEM by counting spherules in 1-μm^2 areas in 10 to 15 images per sample.

RESULTS

Semliki Forest virus RCs arise first at the PM. The mRNA sense genome of alphaviruses is translated in the cytoplasm of infected cells to a large polyprotein, from which four nsPs are generated by autoproteolysis (Fig. 1A). Each of the four nsPs colocalizes in a macromolecular complex responsible for viral genome replication, which also contains newly synthesized RNA (reviewed in reference 48) (Fig. 1B). These replication complexes (RCs) are bulb-shaped membrane invaginations designated spherules (Fig.1Dd). A speculative model of the membrane-bound RC is presented in Fig. 1C. We use the terms RC and spherule as synonyms below.

We wanted to follow the distribution of SFV RCs in a time course, starting from very early time points after infection, in order to detect the first active RCs. For this purpose, BHK cells were infected and fixed starting from 1 h postinfection (p.i.). After fixation, cells were coimmunolabeled with polyclonal antibodies raised against each of the four nsPs (nsP1 to nsP4) and a monoclonal antibody against dsRNA. The presence of dsRNA molecules in infected cells is a hallmark for positive-strand RNA virus genome replication (61). As shown by double labeling with anti-nsP3 and anti-dsRNA antibodies, there was colocalization of these labels throughout infection (Fig. 1D). This was true also for antisera against nsP1, nsP2, and nsP4 (not shown). There was no detectable labeling of mock-infected cells with any of the antibodies (Fig.1Da), and therefore, labeling with an anti-dsRNA antibody was a reliable tool for revealing the RCs. The dsRNA signal was also sharper than that obtained with antibodies against nsPs, possibly because the replication intermediates are located inside the spherules and do not diffuse into the cytoplasm (Fig. 1D). Double labeling early in infection revealed that the RCs were almost exclusively at the PM (Fig. 1Db and c). Electron microscopy in parallel samples confirmed the presence of numerous typical spherules on the cell surface at this stage of infection (Fig.1Dd), strongly suggesting that the PM was the site of formation of these structures. Evidently, the RCs were removed from the PM at later stages of infection. From 2 to 4 h p.i., double labeling with anti-dsRNA and anti-nsP3 antibodies resulted in the staining of small intracellular vesicles (Fig. 1De to g). Interestingly, when the bottom of the cell, where the PM is parallel to the confocal optical plane, was imaged, dsRNA-labeled RCs reproducibly aligned in stripes (Fig.1Df). At 8 h p.i., RCs were detected in typical perinuclear cytopathic vacuoles (CPV-I). No PM staining could be detected at this time point (Fig.1Dh).

To determine whether the localization of RCs depended on the amount of virus used, we infected the cells at two more multiplicities of infection, 5 PFU/cell and 500 PFU/cell. Irrespective of the 100-fold difference in the virus inocula, the dsRNA signal was first detected at the PM, where it was amplified significantly, followed by stepwise internalization during infection, leading finally to accumulation in the perinuclear area (data not shown).

Quantitative analysis of RC localization. The time course experiments clearly illustrated that the localization of the RCs followed a chronological order: first at the PM, then in small and scattered cytoplasmic vesicles, and finally in large perinuclear vacuoles, the previously described CPV-I (1, 15, 28, 44). Our aim was to systematically dissect the main steps of this "cycle" using inhibition studies aimed at blocking the RCs in each of these three stages. For this purpose, three major phenotype groups were visually distinguished (see Materials and Methods) based on the localization of dsRNA: early (PM), intermediate (PM and small cytoplasmic dots), and late (large vacuoles in the perinuclear area) (Fig. 1E). In this and further inhibition experiments, cells were infected using 500 PFU/cell, since a fast and synchronous infection cycle allowed shorter-time-scale experiments. This was important in order to avoid nonspecific effects when cells were exposed to different pharmacological treatments. Under these experimental conditions, more than 60% of the cells had strong dsRNA staining at the PM at 1 h 30 min p.i. During the course of infection, the RC localization shifted toward an intermediate (2 h 30 min p.i.) and then a late (4 h p.i.) phenotype, supporting the idea that

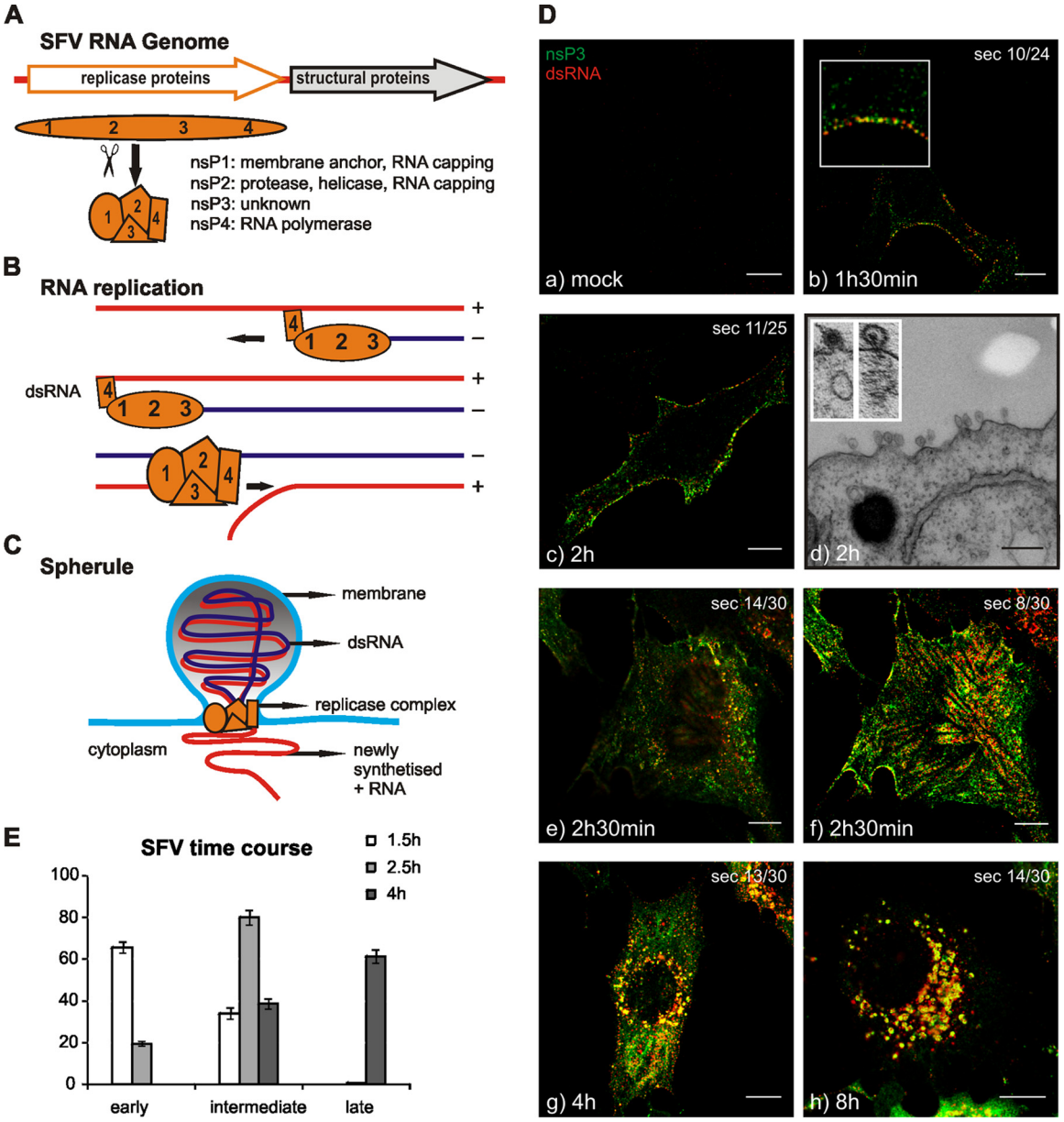

FIG. 1. Replication scheme and time course of SFV infection. (A) Schematic view of the SFV genome and expression of the ns proteins. The main functions of the individual ns proteins are shown. (B) RNA replication strategy of SFV through a dsRNA intermediate. Although the replication intermediate is shown as entirely double stranded, the actual extent of the dsRNA is not known. (C) Model of the replication-induced membrane structure, or spherule, with replicase proteins shown at the neck and a dsRNA molecule located inside the spherule. Newly synthesized positive-sense RNA is released to the cytoplasm. Proteins are not shown to scale. Multiple copies of replication proteins could be located throughout the spherule (24). (D) Localization of SFV RCs in a time course. BHK cells were either mock infected or infected with SFV at 50 PFU/cell, and samples were fixed at the indicated time points p.i. RCs were detected with anti-nsP3 (green) and anti-dsRNA (red) antibodies. Colocalization (yellow) represents active RCs. Samples were analyzed with confocal microscopy, and representative optical sections from the middles of the cells are shown. The total number of sections (sec) per cell is also given. (a) Mock-infected sample. (b and c) Samples fixed at 1 h 30 min (b) and 2 h (c) demonstrate the accumulation of the RCs at the PM. (d) The EM cross section corresponding to panel c shows the spherules at the PM. (Inset) A virus particle at the outer surface of the PM (left) appears similar in size but morphologically distinct from a spherule (right). (e and f) For the sample fixed at 2 h 30 min, both a middle (e) and a bottom (f) section are shown. (g and h) Images of samples fixed at 4 h (g) and 8 h (h) demonstrate the later phenotype with perinuclear CPVs. Bars, 10 μm for confocal microscopy images and 200 nm for the EM image. (E) Visual profiling. Phenotypes were defined according to the localization of RCs in a time course of infection with 500 PFU/cell. Images of 5 fields per coverslip at each time point were randomly selected, and approximately 100 cells were marked in each field. According to the localization pattern of the RCs, the cells were grouped into three phenotype categories: early (PM staining), intermediate (PM staining and small RC-containing vesicles), and late (larger perinuclear RC-containing vesicles [CPV-I]).

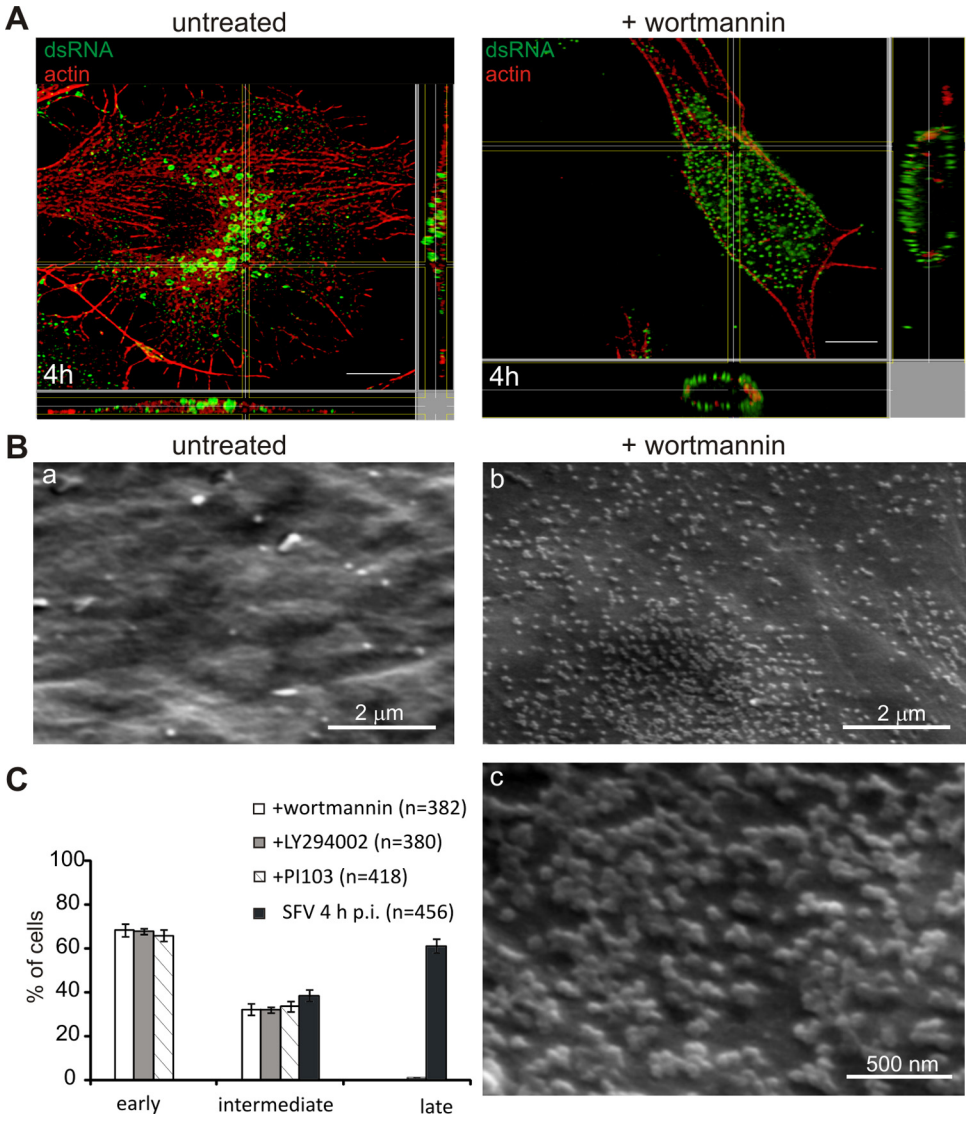

FIG. 2. Involvement of PI3K in the trafficking of the RCs. (A) Wortmannin blocks RCs at the PM. Untreated cells and cells treated with 100 nM wortmannin were analyzed by orthogonal optical sectioning. In the untreated sample, dsRNA-positive CPV (green) are located in the perinuclear area at 4 h p.i., but wortmannin inhibits the internalization of the RCs. Cell contours are shown by staining of actin with phalloidin-AF568 (red). Bars, 10 μm. (B) Parallel samples were analyzed by scanning electron microscopy. (a) An untreated sample shows a clear PM with very few spherules at 4 h p.i. (b) In a wortmannin-treated sample, the PM is filled with spherules. (c) High magnification of an area acquired from an adjacent field of the treated sample, showing that spherules appear in clusters. (C) Quantification of the localization of RCs in the presence of 100 nM wortmannin, 50 μM LY294002, or 200 nM PI-103 compared to the localization of RCs in an untreated sample. Infected cells from four fields (n indicates the total number of the cells analyzed) were quantified for RC localization. Error bars represent SDs.

the CPV-I represent the final stage of RC trafficking, which starts from the PM.

The activity of class I PI3K is needed for the PM internalization of RCs. To demonstrate that the RC spherules found on the surfaces of modified endosomes and lysosomes originate from the PM, a set of drugs was tested for the ability to block internalization. Drugs that induced actin depolymerization (e.g., latrunculins and cytochalasins) could not be used for long experiments, since BHK cell monolayers were very sensitive to such treatments and detached within minutes. Microtubule disruption was much better tolerated but did not stop spherule internalization. Rather, it affected later steps of RC intracellular trafficking (see below). We found that wortmannin, a potent and irreversible inhibitor of PI3K (5), fulfilled the task of retaining the RC spherules at the PM.

After incubation for 1 h 30 min, SFV-infected cells were treated with different concentrations of wortmannin. At 4 h p.i., cells were fixed, and RCs were visualized by dsRNA immunofluorescence labeling. The treatment caused a virtually complete block of the RCs at the PM (Fig. 2A). In control experiments, the presence of wortmannin did not inhibit the clathrin-dependent uptake of transferrin, which accumulated in enlarged cytoplasmic vacuoles, as previously reported (55). To obtain ultrastructural information and to estimate the extent of spherule retention at the PM, drug-treated infected cells were imaged by scanning electron microscopy. The results

confirmed that the PM was covered with thousands of clustered spherules (Fig. 2Bb and c), in contrast to the smooth appearance of untreated infected cells in a parallel experiment (Fig.2Ba). The wortmannin-induced RC retention at the PM was concentration dependent, and a clear effect could be obtained even with 30 nM. Another control experiment was performed by treating uninfected cells with wortmannin. These cells again showed a smooth appearance, confirming that wortmannin by itself does not induce any cell surface structures (data not shown). Quantitative immunofluorescence analysis showed that when a concentration of 100 nM was used, more than 65% of the cells showed a strong dsRNA signal at the PM even at 4 h p.i. (Fig. 2C), resembling the localization of RCs in early stages of infection. These results were also confirmed in murine embryonic fibroblasts (MEFs) and HeLa cells. Notably, when added at the beginning of infection (20 min p.i.), wortmannin did not interfere with the PM targeting of RCs (not shown); dsRNA-positive RCs still targeted the PM, whereas little or no signal was detected in the cytoplasm. To confirm our results, two other PI3K inhibitors were tested. The drug PI-103, a specific inhibitor of class I PI3K, and the less-specific inhibitor LY294002 (5, 24) were used. PI-103 (200 nM) and LY294002 (50 μM) were added at 1 h 30 min p.i., and the cells were fixed at 4 h. The results were comparable to those obtained with wortmannin: the vast majority of the spherules were blocked at the PM (Fig. 2C). Similar results were also observed with MEFs and HeLa cells, showing that the same trafficking route is used in these three different cell lines. For the reversible inhibitor LY294002, we also tested the effect of the removal of the drug. The inhibitor was removed at 4 h p.i., and the incubation was continued up to 8 h p.i. dsRNA staining confirmed that all the RCs were internalized after the washout of the drug and localized perinuclearly (data not shown).

Use of SFV-ZsGreen to follow RCs in live cells. In order to monitor the events that lead the RCs from the PM to the perinuclear area in live cells, a recombinant SFV was created by fusing the coral reef ZsGreen (ZsG) fluorescent protein with the replicase protein nsP3 (Fig. 3A). Since only the viral protein nsP1 has membrane binding activity (3, 56), the colocalization of nsP3-ZsG with membranes in live cells (and with dsRNA in fixed samples) indicates its presence as part of the replication complex. Virus growth rates and the stability of the nsP3-ZsG fusion protein are shown in Fig. 3A. The colocalization of nsP3-ZsG with dsRNA in fixed cells confirmed its participation in the replication complex and the massive accumulation at the PM early in infection (Fig. 3B).

To determine whether the nsP3-ZsG fluorescent signal could be used as an accurate marker to follow the spherules in live cells, we used correlative light-electron microscopy (CLEM) (41, 42). This is a recently developed technique by which a cell of interest is first imaged by fluorescence microscopy and is subsequently localized and analyzed by electron microscopy (see Materials and Methods). BHK cells were infected with SFV-ZsG VRPs (500 infectious units [IU]/cell) and were fixed at 2 h 30 min p.i. In order to visualize only the membrane-bound nsP3-ZsG, the PM adjacent to the coverslip was imaged with confocal fluorescence microscopy (Fig. 3Ca, inset). Samples were then prepared for conventional transmission electron microscopy, and the first section parallel to the coverslip was used for EM imaging. The cell of interest was first relocalized at low magnification (Fig.3Ca). Higher magnifications of this portion of the PM confirmed the presence of thousands of spherules (Fig. 3Cb and c), which reached maximum densities of >100 per μm^2 (the mean density in this region was $74 \pm 41/\mu m^2$ [range, 26 to $132/\mu m^2$]; a total of 1,156 spherules were counted in the experiment) and appeared disconnected from the surrounding cytoplasm as a result of horizontal sectioning.

As in the case of wt SFV-infected cells, at later stages of infection nsP3-ZsG localized at the limiting membranes of large vacuoles concentrated in the perinuclear area and positive for LysoTracker, a marker of acidic organelles (Fig. 3D). Notably, the vast majority of the cellular acidic vacuoles were now completely surrounded by nsP3-ZsG (Fig. 3D). EM analysis of parallel samples confirmed the presence of numerous CPV-I, each harboring hundreds of spherules (not shown).

Intracellular dynamics of RCs. Once it was established that the recombinant SFV-ZsG was a suitable tool, fluorescent live-cell imaging was performed. As a starting point, wide-field imaging was used in order to obtain a general overview of the intracellular dynamics of the RCs.

BHK cells were infected with SFV-ZsG VRPs at 500 IU/cell. Under these conditions, the nsP3-ZsG signal was already detectable at 2 h p.i. LysoTracker was added to simultaneously visualize the cellular acidic compartment. In live-cell imaging, RCs appeared to be associated with very dynamic organelles, which displayed different types of movements. The smallest ZsG-positive intracellular vesicles were more abundant in the cell periphery in the early stages of infection and did not colocalize with LysoTracker. These LysoTracker-negative vesicles underwent multidirectional and short-distance movements (see video S1 in the supplemental material). On the other hand, larger vesicles containing the RCs were always acidic, displayed less-frequent, saltatory movements over long distances (see video S2 in the supplemental material), and underwent multiple fusion and fission events throughout the cytoplasm. In contrast, the largest acidic ZsG-positive vesicles (CPV-I) were immobile and were concentrated in the perinuclear area (see video S3 in the supplemental material).

To obtain more-detailed information about different types of RC movement, particle tracking after confocal live-cell imaging was performed. Early in infection (at 2 h 30 min p.i.), fast, multidirectional movements (type I) of nonacidic RC carriers were dominant (Fig. 4A, tracks 1 to 5), with mean velocities in the range of 0.3 μm/s (Fig. 4C, track A1, and D). However, the displacement of these vesicles remained rather small (2.1 ± 0.5 μm), suggesting an actin-based transport mechanism (22).

On the other hand, RCs that were associated with the acidic organelles showed a different type of dynamic (type II movements). They traveled distances of >10 μm (Fig. 4A, track 6) and showed peak velocities as high as 1.3 μm/s (Fig. 4C, track A6, and D), resembling microtubule-based transport (37). These type II movements continued until the later stages of infection (4 h p.i.), resulting in the perinuclear localization of acidic ZsG-positive organelles (Fig. 4B). At this time point, a third type of dynamic was also seen (type III movement) (Fig. 4B, tracks 1 and 2). Large acidic organelles covered with RCs (CPV-I) in the perinuclear area displayed a very static nature

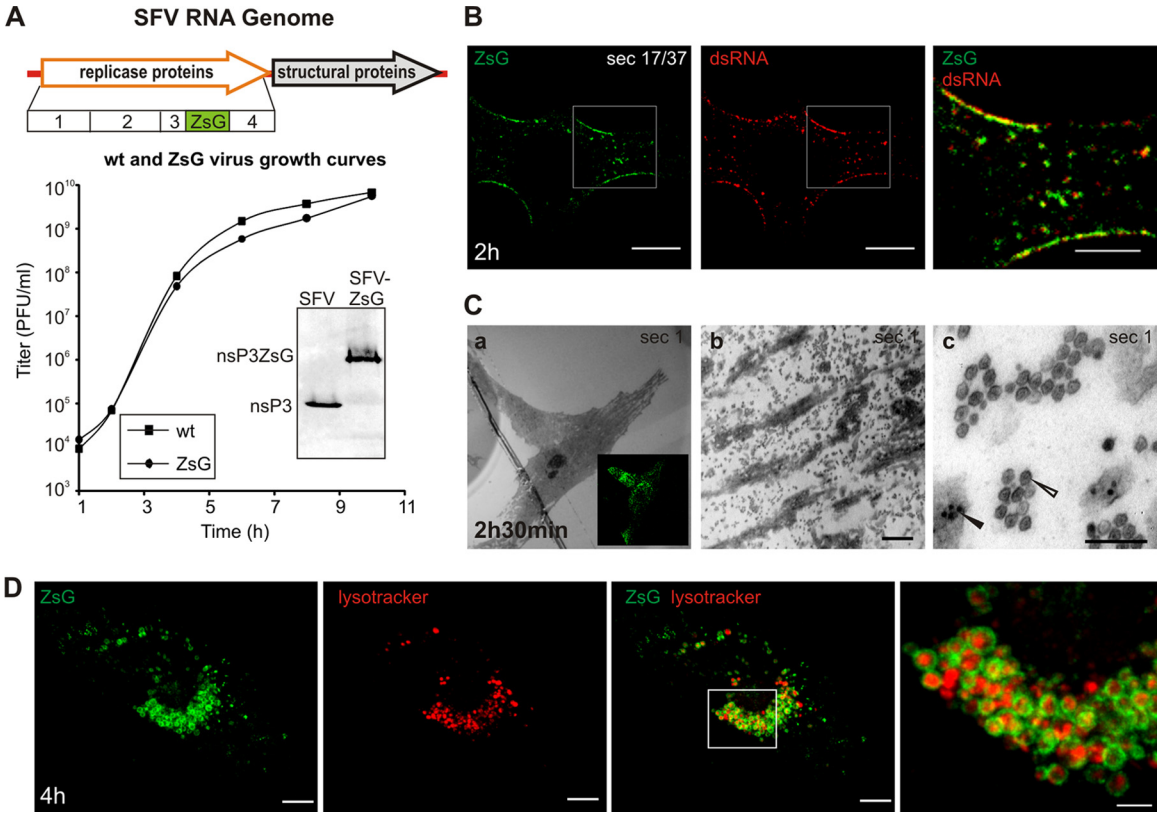

FIG. 3. Analysis of replication of SFV-ZsG in fixed and live cells. (A) (Top) Schematic view of the SFV-ZsG genome. The insertion of the ZsG sequence is highlighted. (Bottom) The growth curve of SFV-ZsG is compared to that of the wt SFV4 virus. BHK cells were infected with 10 PFU/cell, and aliquots were taken every 2 h. Titers (PFU/ml) were determined by a plaque assay. At 10 h, cells were lysed, and samples were analyzed by Western blotting with anti-nsP3 antibodies to verify the presence of the fusion protein nsP3-ZsG (shown in the inset). (B) PM localization of RCs containing ZsG early in infection. BHK cells were infected with SFV-ZsG at 500 PFU/cell and were fixed at 2 h p.i. An anti-dsRNA antibody (red) was used to confirm the presence of ZsG in replication complexes. A representative confocal section is shown. The area that is boxed in the left and center panels is displayed at higher magnification on the right and shows the colocalization of the dsRNA and ZsG signals. Bars, 10 μm (left and center) and 5 μm (right). (C) Correlative light-electron microscopy (CLEM) was used to study the RCs at the bottom of the cell. BHK cells were infected with SFV-ZsG VRPs (MOI, 500), and at 2 h 30 min p.i., cells were fixed with glutaraldehyde. (a) A representative infected cell was imaged with a confocal microscope (inset image in green). The same cell was relocated by EM, and the first horizontal section (sec 1) was analyzed. (b) A higher magnification of the same cell shows massive amounts of spherules at the bottom of the cell. Bar, 1 μm. (c) Higher magnification of panel b, showing clusters of spherules (white arrowhead) distinct from the nucleocapsids (black arrowhead). Bar, 200 nm. (D) Live-cell imaging of BHK cells infected with SFV-ZsG VRPs (MOI, 500). The cellular acidic compartment was visualized by LysoTracker (red). Images were captured at 4 h p.i. with confocal microscopy. 3D reconstruction of the entire cell is shown (see Materials and Methods). Bars, 10 μm (left and central panels) and 3 μm (rightmost panel).

(Fig. 4C, track B1, and D; see also video S3 in the supplemental material).

Fusion events leading to different types of dynamics of RC carriers, from type I to type III movements, were followed at 3 h p.i. Fast fusion events occurred between small neutral ZsG-positive vesicles and larger acidic organelles. This type of event was followed by directional transport to the perinuclear area (Fig. 4E, arrowheads; see also video S4 in the supplemental material), representing type II movement. Slow fusion events between acidic ZsG-positive organelles could also be detected, resulting in large organelles that progressively lost their dynamics (Fig. 4E, circled areas; see also video S4 in the supplemental material), illustrating type III movements. These results suggest a mechanism for the biogenesis of the CPV-I in which RCs, internalized from the PM in small neutral vesicles, are delivered to larger acidic organelles as a result of multiple fusion events and are transported to the perinuclear region.

An intact actin-myosin network is required at the early stages of RC trafficking. Actin plays an important role during endocytosis and vesicle transport (16, 54). In mammalian cells, for instance, this cytoskeleton component is involved in different stages of both clathrin- and caveola-mediated endocytosis, although a complete description of the molecular events regulating this process is still missing. The contribution of the actin network to the early events of RC trafficking was investigated. As shown in Fig.1Df, the RCs labeled with an anti-dsRNA antibody were not randomly distributed but were strongly aligned in stripes at 2 h 30 min p.i. This phenomenon is reproducible (44) and is more evident when one is imaging the PM attached to the coverslip, where the actin network is very abundant. Therefore, infected BHK cells were costained with anti-dsRNA (or anti-nsP3) and phalloidin to visualize the possible connection between viral replicase and actin fibers, respectively. Although no colocalization could be detected

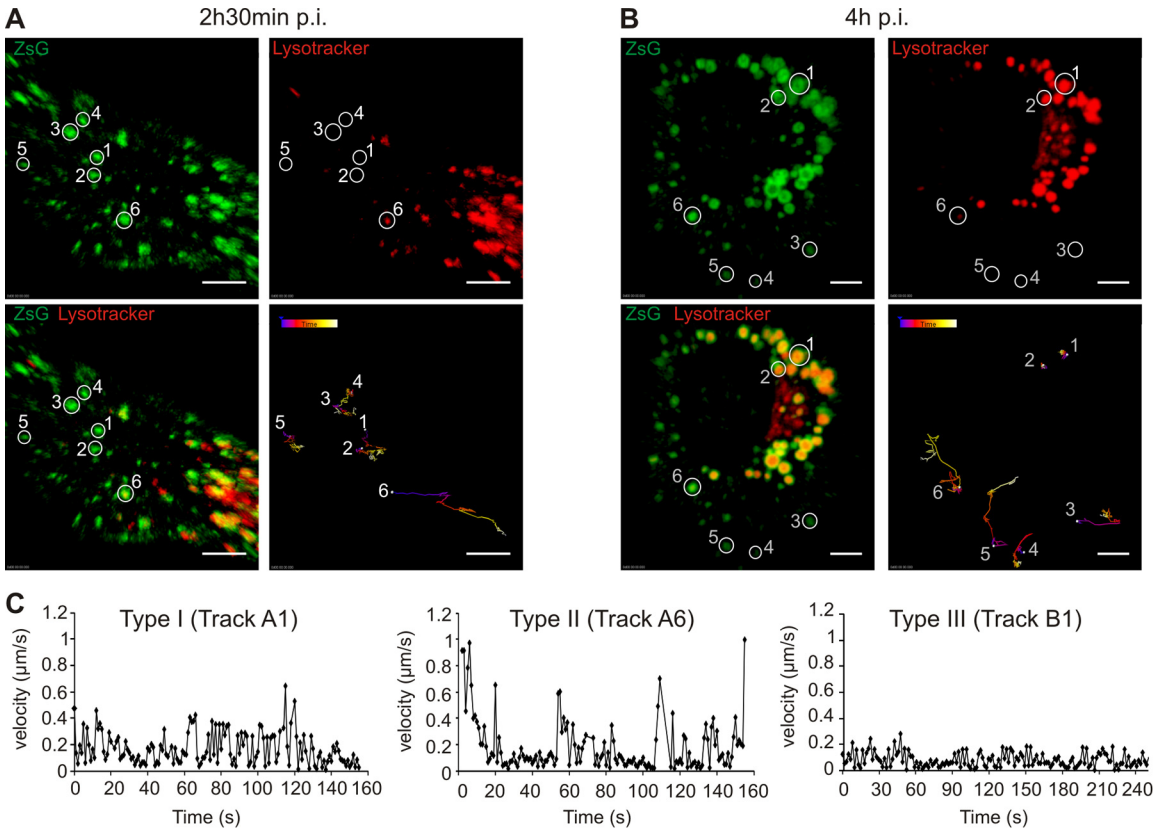

D

	Type I	Type II	Type III
Track displacement (µm)	2,1 ± 0,5	10,1 ± 1,6	0,8 ± 0,3
Max velocity (µm/s)	0,65 ± 0,14	0,99 ± 0,3	0,21 ± 0,07
Mean velocity (µm/s)	0,3 ± 0,01	0,19 ± 0,04	0,1 ± 0,05

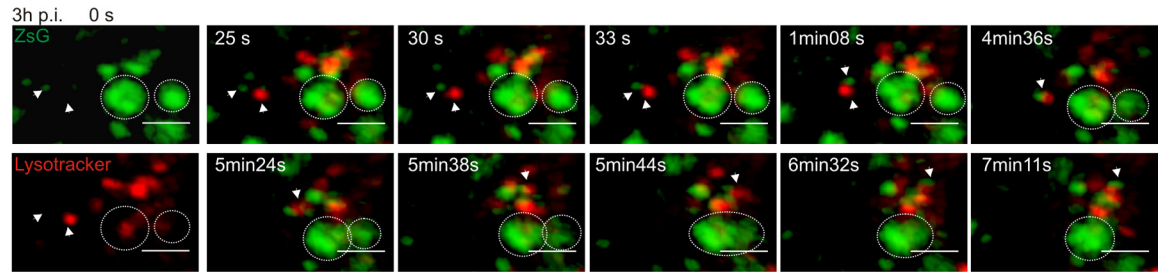

FIG. 4. Intracellular dynamics of RCs at different stages of infection. (A and B) Confocal live-cell imaging of BHK cells infected with SFV-ZSG VRPs (MOI, 500). LysoTracker (red) highlights the acidic cellular organelles. The tracking of six ZsG-positive vesicles is shown. The respective vesicles are circled in split channels (at the top) and also in the merged image (bottom left); these images represent the first frame of the recording. Tracks are color coded according to time, as indicated on the images. Bars, 5 µm. The rate of the recording was 0.5 frame/s (0.5 Hz). (A) Different dynamics of RCs early in infection (2 h 30 min p.i.). Tracks 1 to 5 represent type I movements, and track 6 represents type II movements. Note that only vesicle 6 is acidic. The total recording time was 5 min 21 s. (B) Dynamics of RCs late in infection (4 h p.i.). Tracks 1 and 2 (type III) show the movements of late acidic ZsG-positive vesicles (CPV-I), which are mostly immobile. Tracks 3 and 4 show the movements of small RC-containing vesicles that are not acidic (type I), and tracks 5 and 6 demonstrate directed long-distance type II dynamics. Vesicle 5 becomes acidified during the recording, and vesicle 6 is already acidic at the beginning of the movie (see video S3 in the supplemental material). The total recording time was 4 min 40 s. (C) Representative track charts for type I (track A1), type II (track A6), and type III (track B1) movements. The changes in velocity during the recordings are shown. (D) Summary table of the three types of movements of RC-positive vesicles during the SFV infection cycle. Track displacement and maximum and mean velocities are shown; SDs were calculated based on six tracks. (E) Live-cell imaging of BHK cells infected with SFV-ZSG VRPs (MOI, 500) at 3 h p.i. (see video S4 in the supplemental material). LysoTracker (red) highlights the cellular acidic organelles. The frames were recorded at the rate of 1 frame/s (1 Hz) over 7 min 35 s. Split channels are shown at time zero (left top and bottom panels); otherwise, merged images are presented. The fast fusion of an early ZsG-positive vesicle (not acidic) with a preexisting acidic organelle is indicated by arrowheads, and its long-distance movement to the pericentriolar area is followed. In the same movie, the slow fusion of two CPVs is indicated by circled areas. Bars, 3 µm.

with the stress fibers that were more strongly stained by phalloidin, at 2 h 30 min p.i. the striped pattern of nsP3 distribution followed the direction of the actin fibers (Fig. 5A). This was especially evident at higher magnifications (Fig. 5A, rightmost panel). Microtubules did not follow the striped pattern of RCs at this time of infection (not shown). Pharmacological inhibition studies confirmed a role for the actin network during the early stages of RC trafficking. To test whether interference with the dynamics of the actin network affected the movement of the RCs, we used blebbistatin, an inhibitor of the actin motor protein myosin II (26, 57). BHK cells were infected with SFV-ZsG VRPs (500 IU/cell) for 2 h 30 min, followed by exposure to blebbistatin (30 nM) for 2 or 10 min before imaging. Strikingly, even the smallest RC-containing vesicles were immobile, as shown by particle tracking (Fig. 5B), in contrast to the highly dynamic movements detected by vesicle tracking in untreated cells (compare Fig. 4A). In Fig. 5C, different parameters of vesicle motion are reported for cells exposed to blebbistatin for 2 or 10 min (compare with values in Fig. 4C and D).

When RCs were allowed to accumulate at the PM in the absence of drugs for 1 h 30 min, the addition of blebbistatin caused a significant delay in the internalization of RCs. Even at 4 h p.i., many cells had strong PM staining, with only few small cytoplasmic dots (Fig. 5D, dsRNA). This long exposure to the drug resulted in depolymerization of the actin fibers (Fig. 5D, actin). Consistently, the striped pattern of the RCs was lost. Quantification showed that at this time point, only 11% of the cells had the late phenotype in the presence of blebbistatin (Fig. 5E), compared to 65% in the untreated sample.

The alignment of RCs and actin fibers was detected only early in infection. It has been reported previously that at late time points SFV leads to the disruption of the actin cytoskeleton. This is caused by the viral protein nsP1 through an unknown mechanism (29). Interestingly, we found a strong correlation between the localization of RCs and the stage of actin disruption (Fig. 5A and F). When the RCs were still aligned in stripes, the actin fibers were intact. As the RCs moved inward, the actin started to be destroyed. By 6 h p.i., when all the replication complexes localized in the perinuclear area, no actin fibers could be detected by phalloidin staining. Instead, very prominent filopodium-like extensions that were positive for actin were induced (Fig. 5F). Taken together, these results suggest an important role for actin only at the early stages of RC trafficking.

Microtubules and the biogenesis of the CPV-I. Wide-field live-cell imaging recordings and speed measurements after confocal microscopy indicated that the directed long-distance movements of RC carriers were consistent with microtubule-dependent transport (Fig. 4A to D, type II movements) (37, 63). Moreover, at 4 h p.i., CPV-I systematically accumulated around the centrioles and surrounded the Golgi apparatus in interphase cells, in a ring-like arrangement (not shown).

To investigate the role of microtubules, the microtubule network was disrupted by the addition of nocodazole (5 μM) to BHK cells together with SFV or SFV-ZsG VRPs (500 PFU/cell), since it has been shown previously that the entry of SFV is not dependent on microtubules (59). Acidic organelles were labeled by the addition of LysoTracker 20 min before live-cell imaging. At 4 h p.i., untreated cells infected with SFV showed a typical pattern of large CPV-I in the perinuclear area (Fig. 6A). Higher magnification and 3D reconstruction revealed that nsP3-ZsG-labeled RCs were actually surrounding the acidic lumen of the CPV-I. EM analysis in parallel experiments confirmed the presence of numerous CPV-I in the perinuclear region, each having a diameter of 400 to 600 nm and a high density of spherules at the limiting membrane (see Fig. 8 for an overview of RCs at various stages of infection).

A completely different pattern was seen in nocodazole-treated infected cells. The RCs were associated mostly with smaller vesicles that were not stained with LysoTracker. These vesicles were scattered throughout the cytoplasm (Fig. 6B). Some of the acidic organelles were also positive for nsP3-ZsG, but, as shown by 3D modeling, RCs appeared only as a few sparse patches and no longer saturated the limiting membranes of these enlarged acidic vacuoles (Fig. 6B, right). EM analysis in separate experiments confirmed the presence of two populations of spherule-containing vacuoles in nocodazole-treated samples. The smaller vacuoles often had a diameter of 250 to 350 nm and had numerous spherules at 4 h p.i.; the larger vacuoles ranged from 600 to 800 nm in diameter and had sparse spherules on their limiting membranes (not shown).

Tracking of the RC movement after confocal microscopy showed that in the presence of nocodazole, the type II movement described above was inhibited (Fig. 6C). Although the microtubule network was completely destroyed by nocodazole, at 2 h p.i. RCs showed PM localization, and the characteristic stripes at the bottom of the cell remained aligned with actin fibers (not shown). Confocal imaging also showed that most of the nsP3-positive structures were positive for dsRNA, demonstrating that nocodazole does not interfere either with spherule formation at the PM, with RNA replication (as assessed by dsRNA staining), or with the internalization of the viral RNA replication complexes (Fig. 6D). Instead, nocodazole affected the further transport of the internalized small vesicles carrying spherules, resulting in their scattered distribution all over the cytoplasm.

Taken together, these results are in agreement with the model that microtubule-based movement serves as a mechanism to transport the spherules from the small neutral vesicles to the surfaces of acidic organelles. In the absence of nocodazole, this process culminates in the formation of the typical, large CPV-I, which accumulate in the pericentriolar area.

Virus replication in the presence of inhibitors of RC trafficking. Virus production and RNA synthesis were measured in the presence of wortmannin or nocodazole, which stopped the RCs at the PM or at small cytoplasmic vesicles, respectively. After a 1-h infection with SFV-ZsG (MOI, 10), BHK cells were treated with the different drugs, and released viruses were collected at 2-h intervals. Drugs were replenished after each withdrawal. A one-step growth curve was obtained for each sample as explained in Materials and Methods. As shown in Fig. 7, the stopping of RCs at the PM by wortmannin treatment did not inhibit virus production. In contrast, microtubule disruption decreased the level of virus release more than 10-fold. The effects of the drug treatments on viral RNA synthesis were also tested (Fig. 7, inset). While in the presence of wortmannin, RNA production was significantly higher than that of untreated infected cells, nocodazole had a slight inhibitory effect. Thus, spherules at the PM are active in RNA

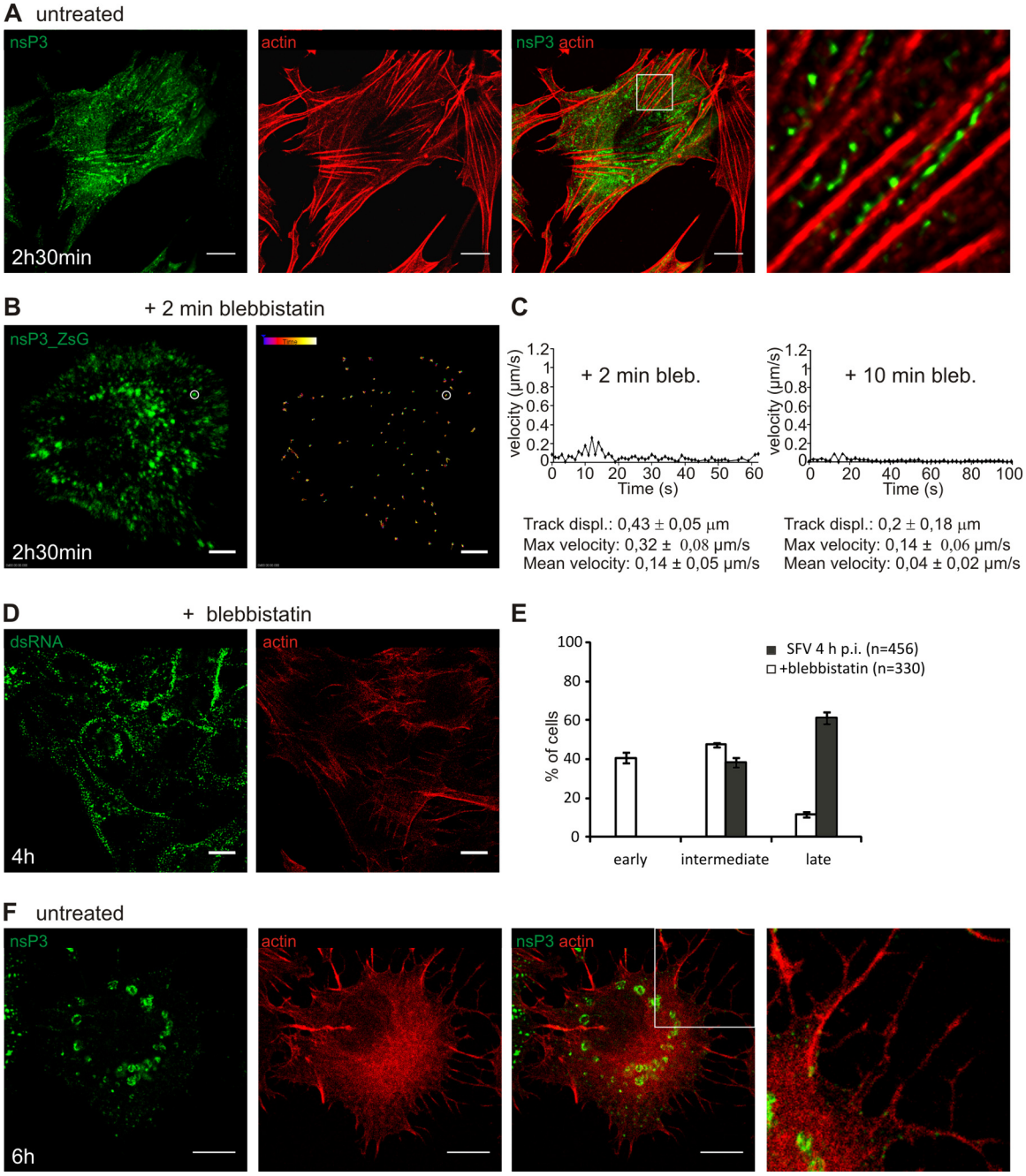

FIG. 5. The actin network is utilized early in infection. (A) RCs are aligned at the bottom of the cell following the direction of actin fibers. BHK cells were infected with SFV (MOI, 50) and were fixed at 2 h 30 min p.i. RCs were stained with an anti-nsP3 antibody (green), and actin was visualized with phalloidin-AF568 (red). Bar, 10 μm. The boxed area is shown at a higher magnification in the rightmost panel. (B) Blebbistatin freezes all the movements of RCs in live cells. BHK cells were infected with SFV-ZsG VRPs (MOI, 500), and 30 nM blebbistatin was added at 2 h 30 min p.i. Imaging was started 2 min after the addition of the drug. Representative tracks are shown (image on the right). The rate of the recording was 0.5 frame/s (0.5 Hz). The total recording time was 3 min 44 s. Images represent the first frame of the recording. Bar, 5 μm. (C) (Left) Track of the vesicle circled in panel B (after exposure to blebbistatin for 2 min). (Right) Illustrative track from a 10-min treatment with blebbistatin. Under the graphs, statistics for six representative tracks are shown. (D) Blebbistatin treatment delays the inward movement of the RCs and the maturation of the CPV. BHK cells were infected with SFV (MOI, 500), and 30 nM blebbistatin was added at 1 h 30 min p.i. Samples were fixed at 4 h p.i. and were stained with an anti-dsRNA antibody (green) and phalloidin-AF568 (red). (E) The localization of the RCs was quantified in four fields (n indicates the total number of the cells analyzed) and was compared to that in an untreated sample. Error bars represent SDs for two independent experiments. (F) Actin disruption later in infection. BHK cells were infected with SFV (MOI, 50) and were fixed at 6 h p.i. The sample was stained as described for panel A. The boxed area is shown at a higher magnification in the rightmost panel, displaying the virus-induced filopodium-like extensions that contain actin. Bars, 10 μm.

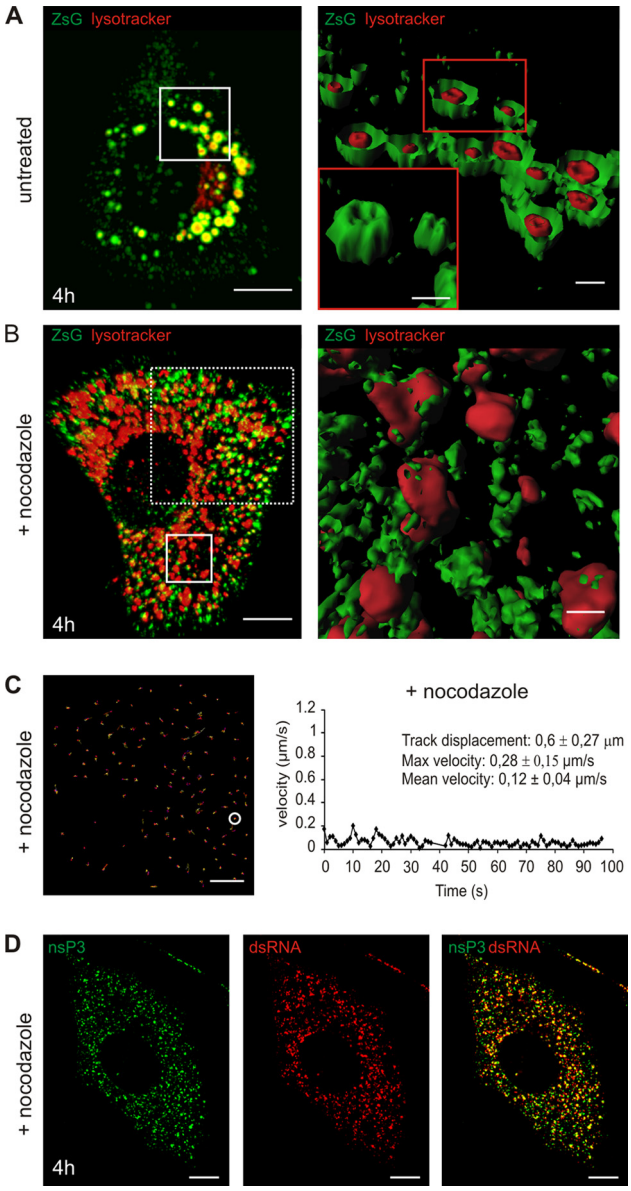

FIG. 6. Involvement of microtubules in the transport of CPV to the perinuclear area. (A to C) Confocal live-cell imaging of SFV-infected cells, either untreated or in the presence of nocodazole (from the beginning of infection). BHK cells were infected with SFV-ZsG VRPs (MOI, 500), and imaging was performed at 4 h p.i. LysoTracker (red) was used to stain the acidic organelles. (A) (Left) Untreated sample, showing the late phenotype and the ZsG signal around the acidic organelles. (Right) Isosurface representation of the area boxed on the left. CPV were cut in half to illustrate the ZsG signal surrounding the LysoTracker staining. (Inset) Intact CPV in the boxed area, hiding the LysoTracker signal. (B) (Left) In the presence of nocodazole, RC-containing vesicles stay scattered. They are not transported to the perinuclear area, and only some ZsG signal colocalizes with LysoTracker as small patches on the surfaces of acidic organelles. The area boxed with solid lines was chosen for isosurface representation, while the area boxed with dashed lines was used for tracking of the RCs in panel C. Bar, 10 µm. (Right) Isosurface representation. Bar, 1 µm. (C) Tracking of the RCs in a nocodazole-treated sample. The rate of the recording was 0.5 frame/s (0.5 Hz). The total recording time was 1 min 36 s. Representative tracks are shown; statistics for one track (circled) are given on the right. Bar, 5 µm. (D) Nocodazole treatment does not interfere with the replication of SFV. BHK cells were infected with SFV (MOI, 500) in the presence of nocodazole, and cells were fixed at 4 h p.i. The scattered nsP3-positive vesicles (green) are also positive for dsRNA staining (red). Bars, 10 µm.

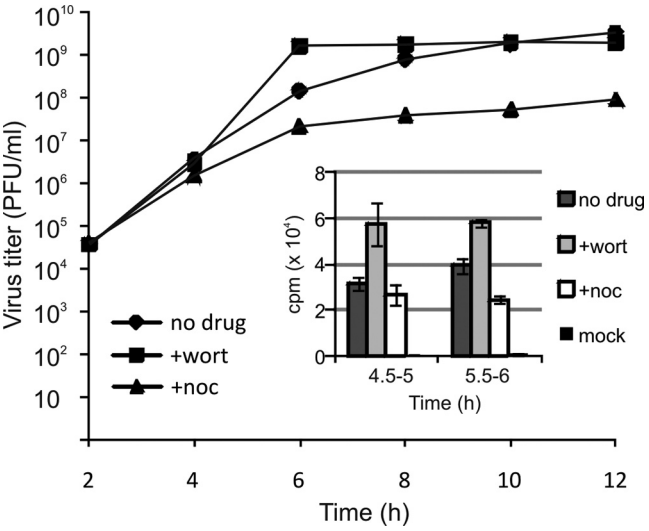

FIG. 7. Virus replication in the presence of inhibitors. One step growth curves of SFV-ZsG in the presence of wortmannin or nocodazole are shown. Released viruses were withdrawn at 2-h intervals as indicated, and virus titers were measured by direct fluorescence (see Materials and Methods). (Inset) Effects of the same inhibitors on SFV RNA synthesis. Infected BHK cells were pulse-labeled with [^{3}H]uridine at the indicated times, and labeled RNA was measured by scintillation counting after TCA precipitation. The results are averages for two independent experiments; error bars represent SDs.

synthesis and sustain virus production similarly to spherules on the CPV. Disruption of microtubules had a small negative effect on RNA synthesis and a larger effect on virion release.

DISCUSSION

All positive-strand RNA viruses studied usurp and modify cytoplasmic membranes, creating characteristic compartments devoted to virus genome replication. The molecular mechanisms that orchestrate the biogenesis and maturation of these complex structures are still poorly understood. The *Togaviridae* (alphaviruses and rubella virus) are so far the only group of viruses known to replicate their genome utilizing endosomal and lysosomal membranes (15, 27). During alphavirus infection, the viral ns proteins and newly synthesized RNA colocalize in membrane invaginations called spherules, which have therefore been identified as the units of RNA replication (21). Their homogenous size and defined morphology makes their recognition by transmission electron microscopy easy, leading to their initial discovery more than 40 years ago (see the introduction). The spherules have a diameter of approximately 50 nm and are connected to the cytoplasm by a pore with a diameter of about 5 to 10 nm (15, 44). Cellular proteins may also participate in these structures (2, 6, 36, 40, 43, 48, 60). Indirect data obtained by studying alphavirus RNA synthesis indicate that the RCs are very stable entities. Minus-strand templates are made only early in infection and remain stable thereafter. Similarly, the positive-strand RNA synthesis rate remains stable for several hours, even in the presence of protein synthesis inhibitors (21). Using live-cell imaging, we provide here the first dynamic view of alphavirus RCs, showing that they undergo an unprecedented large-scale movement.

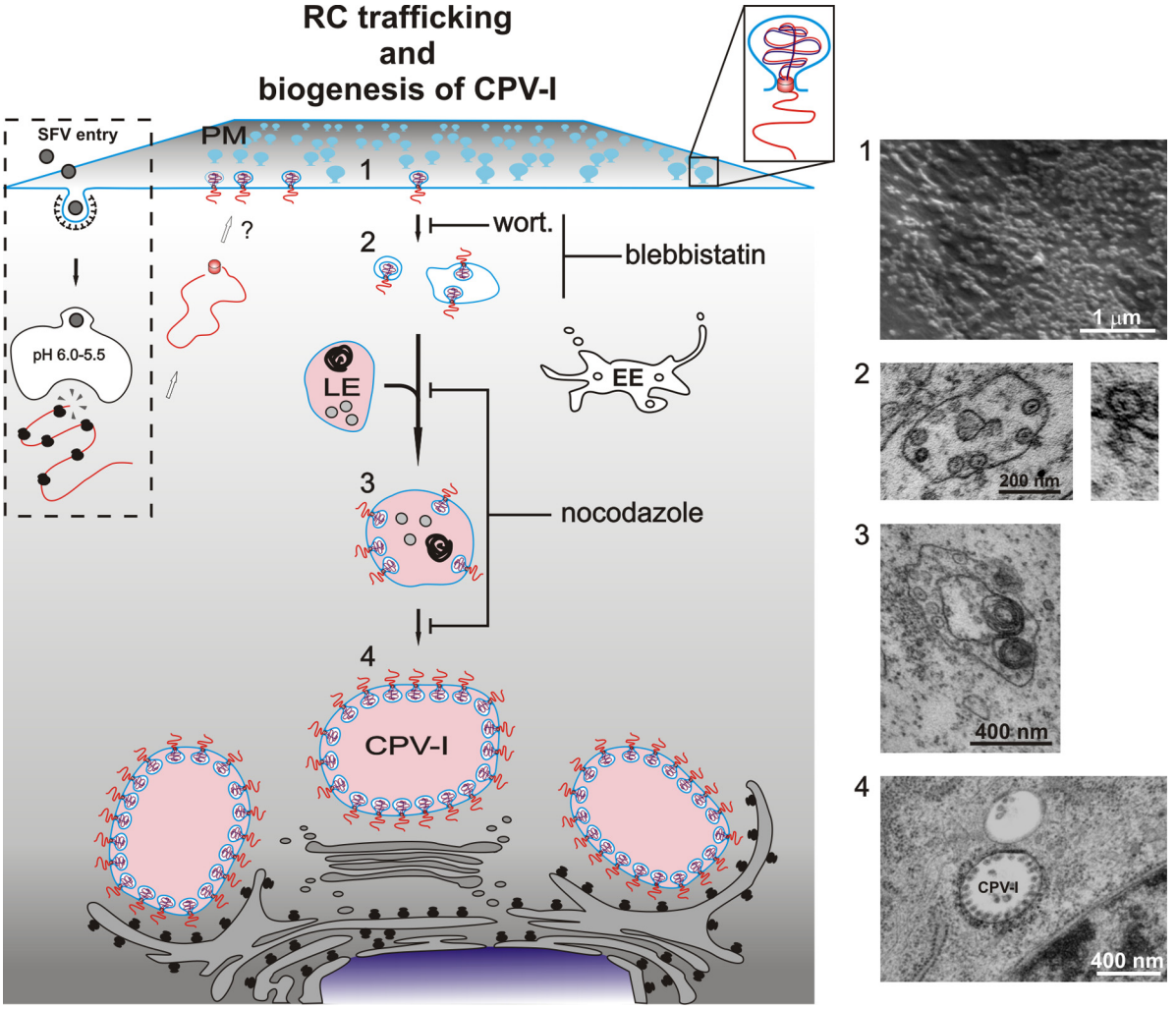

FIG. 8. Model for the trafficking of alphavirus RCs and the biogenesis of CPV-I. After SFV entry, which occurs via clathrin-mediated endocytosis, low-pH-triggered fusion releases the nucleocapsids, and viral mRNA is translated into a polyprotein. Protein-RNA complexes are transported to the PM by an unknown mechanism (white arrows). At the PM, spherule structures are formed (step 1), followed by endocytosis in a PI3K (inhibition by wortmannin)- and actin-myosin (inhibition by blebbistatin)-dependent manner. Small internalized vesicles carry a few spherules (step 2), and many homotypic fusions, as well as fusions with late endosomes, occur (step 3 [inhibition by nocodazole]). These larger, acidic, RC-containing vesicles are transported to the perinuclear area by using microtubules (inhibition by nocodazole), where the maturation of stable large CPV-I is completed (step 4). The acidic nature of the late vesicles is indicated by pink coloring. wort., wortmannin; EE, early endosome; LE, late endosome. Representative EM images from each step of the RC trafficking are shown to the right of the model.

The spherules arise at the PM, from which they are transported to the surfaces of large acidic vacuoles (CPV-I) by means of a specific endocytic event and different components of the cytoskeleton. Using inhibition studies together with quantitative image analysis, we were able to break this pathway into defined stages.

Alphavirus RCs at the PM: accumulation and endocytosis. The early events during virus infection are difficult to monitor, because the initial numbers of RCs are low. However, alphavirus replication is very efficient, and a relatively large virus dose (50 to 500 PFU/cell) was utilized in the current studies. We first detected nsPs and dsRNA at the PM. Discernible signals appeared there by 45 min p.i. and became easily detectable by 1 h 30 min (Fig. 1D). The continued accumulation of a fluorescent signal at the PM was correlated in time and place with the appearance of numerous spherules by using CLEM (Fig. 3C). This experiment, together with previous studies (28), further reinforces the view that the induced membrane alterations are indeed the sites of dsRNA accumulation, and thus, both dsDNA and spherules can be used as markers of the RCs. From the PM, we followed the RCs in live cells by using a recombinant SFV expressing fluorescent hybrid protein nsP3-ZsG, together with continued reference to dsRNA staining and EM experiments. nsP3 appears to be a good marker for the RCs. nsP3 does not contain membrane binding domains; therefore, its association with trafficking vesicles indicates participation in the RC. In particular, nsP3, when expressed alone, is never found at the PM (49), which represents the prominent initial site of RC formation in the current results.

Figure 8 provides an overall summary of our results. Early in infection, even in the absence of inhibitors, the spherules are present at the PM in large quantities, reaching maximal local

densities higher than 100/μm^2. We have not investigated how the newly translated nsPs and the primary RNA template are delivered to the PM before spherule formation. Potentially, the spherule components could arrive there through passive diffusion or active transport in the cytoplasm. The current data show that microtubule-mediated transport and PI3K activity are not involved in the formation of the spherules at the PM, since the addition of nocodazole or wortmannin simultaneously with infection does not inhibit this process. The accumulation of RCs first at the PM probably extends to the whole alphavirus superfamily, since a strong accumulation of dsRNA and replicase proteins at the PM during the early stages of infection has also been seen for cells infected with SIN, another alphavirus rather distantly related to SFV (17, 32).

In order to be internalized, the membranous RCs must utilize an endocytic process. The term internalization, which we have used throughout this work, may not be entirely accurate in this case, since the spherules can already be considered to be internal structures of the cell. The interior of the spherule always remains connected to the cytoplasm through an open neck, and the membrane of the spherule is continuous with the PM and with the limiting membrane of its endocytic carrier vesicle (Fig. 8, step 2). In terms of endocytosis, the spherule can be considered an atypical cargo. Indeed, using EM, our group and others have previously reported the presence of spherules inside PM processes morphologically similar to endocytic vesicles at the stage of internalization (15, 28). We discovered that the primary transfer of spherules from the PM to the cytoplasm requires the dynamics of the actin-myosin network (Fig. 5) and also the activity of class I PI3K (Fig. 2).

By modifying the phosphoinositide composition of intracellular membranes (34), the class I PI3Ks produce second messengers that play a crucial regulatory role in different cellular processes, including endocytosis, cell growth and differentiation, apoptosis, and innate as well as adaptive immune responses (20). Viruses have evolved different strategies to modulate the activities of these enzymes and thereby to regulate different steps during their life cycle, from entry and replication (39, 47, 53) to the tuning of host antiviral responses (7, 9). This work is the first reported study in which PI3K activation was correlated with the localization of the virus RCs. Notably, since spherules have time to accumulate at the PM during the first hours of infection, it is possible that during the internalization stage, the class I PI3K needs to be activated by a specific signal that remains to be characterized. In fibroblasts, the binding of extracellular ligands (e.g., growth factors or viruses) to their receptors leads to a cascade of events that results in the activation of PI3K and the recruitment of proteins involved in actin remodeling (38, 58). Importantly, these events trigger a global activation signal that spreads over the entire surface of the cell. Our results are consistent with the participation of both actin and PI3K in alphavirus RC endocytosis.

One question that arises is which set of molecules triggers the internalization of spherules from the PM, and what role the nsPs play in this process. Studies in which different ns polyproteins were expressed in cell cultures suggest that nsP3 contains at least some of the information required to shift the replicase polyprotein from the PM to the surfaces of endosomes, since polyprotein P12 is found exclusively at the PM, but P123 is also found on endosomes (49). A speculative interpretation is that alphaviruses may have evolved a way to activate the PI3K signaling pathway by first accumulating their RCs at the PM. Our further studies are especially focused on the characterization of the molecular events at the PM and the endocytic pathway utilized for spherule internalization (unpublished data).

Dynamics of viral RCs. Our study provides the first detailed description of the sequential stages of alphavirus RC transport. As summarized in Fig. 8, after their initial massive accumulation at the PM (step 1), SFV spherules are internalized as part of the limiting membranes of small neutral carrier vesicles (step 2). These primary carriers are distributed in the cytoplasm at the periphery of the cell and undergo short-distance multidirectional movement (see video S1 in the supplemental material). We were able to block these movements with blebbistatin, a drug that interferes with the functioning of the actin-myosin network by inhibiting nonmuscle myosin II. After docking with preexisting acidic vesicles, the primary carrier vesicles move rapidly to the perinuclear area close to the microtubule organizing center (MTOC) by directional microtubule-based transport (Fig. 8, step 3), as demonstrated by live-cell imaging (see videos S2 and S4 in the supplemental material) and nocodazole treatment (Fig. 6). In the pericentriolar region, further fusion events generate the final stable and static compartment, the CPV-I (Fig. 8, step 4; see also video S4 in the supplemental material).

To date, the number of studies on RC dynamics in other positive-sense RNA viruses is limited (10, 12, 19, 63). Although our study highlights important differences in the pathways that lead to the modified membrane structures in cells infected by different positive-sense RNA viruses, fundamental similarities are also evident. The replication of hepatitis C virus (HCV) and mouse hepatitis virus (MHV), a coronavirus, occurs on ER-derived membrane structures, which, however, are morphologically quite different for these two viruses. In the studies of RC dynamics, in both instances small, highly mobile structures were reported, which contrasted with the immobile larger accumulations of RCs in the perinuclear area (19, 63). The mobile elements moving along microtubule tracks may represent newly formed RC vesicles. In the case of HCV, it is interesting that although the long-distance movements were independent of the ER, the small RCs were always targeted back to ER tubules (63). The RCs of both HCV and MHV remain on ER-derived membranes and do not proceed, e.g., to the Golgi complex. It was suggested that the small RC-containing elements may coalesce into a reticulovesicular network or a membranous web and may thus be immobilized. For poliovirus, vesicle clusters originating at the ER appear to make use of the components of the cellular anterograde membrane traffic system and also to move along microtubules to a stable perinuclear location (12).

In contrast to these ER-derived RCs, in this study we demonstrate that alphavirus RCs originate at the PM and undergo a multistep vesicular transport pathway, which includes numerous fusion events. The result for alphaviruses is not the formation of vesicular networks but the formation of large acidic vacuoles in the perinuclear area, the CPV-I, containing hundreds of RCs on their surfaces (18). Notably, the average diameter of CPV-I reaches 2 μm at 12 h p.i. (18), significantly

exceeding the sizes of late endosomes and lysosomes in uninfected cells (35). It thus appears that alphaviruses have evolved a mechanism to stabilize membranes of the endolysosomal compartment for their replication.

In spite of these entirely different pathways, a common feature for these positive-strand animal RNA viruses is that the virus-induced membrane rearrangements progressively concentrated around the MTOC. Furthermore, they are quite stable, sustain virus RNA replication for many hours, do not exchange viral proteins with the cytoplasm (19, 63), and appear static when analyzed by live-cell imaging. Thus, HCV and MHV must also disrupt the normal ER dynamics, which would quickly break down the stable membranous webs. The initial mobility of RCs, described for the positive-strand RNA viruses mentioned above and for alphaviruses, may be important in establishing the unusually stable compartments, which remain active in replication for long periods and appear to be resistant to normal cellular mechanisms preventing the accumulation of such structures in uninfected cells. Another interesting similarity is that at least under cell culture conditions, the movements of viral RCs are not strictly required for RNA replication and virus production. Disruption of microtubules with nocodazole has had either no effect or only modest effects on the viruses with which it has been studied (12, 19). With SFV, the retention of RCs at the PM by wortmannin also had no inhibitory effect on virus production or RNA synthesis in cell culture (Fig. 7). Microtubule disruption did have a negative effect on virus release, which was expected, since the transport of envelope glycoproteins to the PM requires microtubule-based anterograde transport (8). The effect on RNA synthesis was less pronounced, and we do not have an immediate explanation for it.

The question of why the alphavirus RCs initially assemble at the PM and are subsequently internalized from there currently remains a matter of speculation. The removal of spherules from the PM is not due to "unspecific" endocytosis, since it requires the activity of class I PI3K, a highly regulated enzyme involved in many different cellular processes. Thousands of spherules are internalized within 2 h, suggesting that this event could result in the modification of large areas of the PM, which plays multiple crucial roles during alphavirus infection. Not only is it the site of virus entry, budding, and, as shown in this work, RC formation, but it also represents the interface between infected cells and cells of the immune system. Thus, the dynamics of alphavirus RCs could also be linked to virus pathogenesis. More insight into the molecular details of this yet unexplored area of alphavirus-host interaction should be gained, and *in vivo* studies will be required to test this possibility.

ACKNOWLEDGMENTS

We thank Johan Peränen and Marja Makarow for critical reading of the manuscript and Andres Merits for providing plasmid pSFV4-ZsG. We are grateful to Pekka Lappalainen and Maria Vartiainen for kindly providing reagents and for advice. We thank Mervi Lindman for technical assistance in EM experiments.

This work was supported by the Academy of Finland (grant 127214) and the Sigrid Jusélius Foundation. P.S. was supported by a fellowship from the Viikki Graduate School in Molecular Biosciences, and G.B. was supported in part by a grant from the Emil Aaltonen Foundation.

REFERENCES

1. **Acheson, N. H., and I. Tamm.** 1967. Replication of Semliki Forest virus: an electron microscopic study. Virology **32:**128–143.
2. **Ahlquist, P., A. O. Noueiry, W. M. Lee, D. B. Kushner, and B. T. Dye.** 2003. Host factors in positive-strand RNA virus genome replication. J. Virol. **77:**8181–8186.
3. **Ahola, T., P. Kujala, M. Tuittila, T. Blom, P. Laakkonen, A. Hinkkanen, and P. Auvinen.** 2000. Effects of palmitoylation of replicase protein nsP1 on alphavirus infection. J. Virol. **74:**6725–6733.
4. **Ahola, T., A. Lampio, P. Auvinen, and L. Kääriäinen.** 1999. Semliki Forest virus mRNA capping enzyme requires association with anionic membrane phospholipids for activity. EMBO J. **18:**3164–3172.
5. **Bain, J., L. Plater, M. Elliott, N. Shpiro, C. J. Hastie, H. McLauchlan, I. Klevernic, J. S. Arthur, D. R. Alessi, and P. Cohen.** 2007. The selectivity of protein kinase inhibitors: a further update. Biochem. J. **408:**297–315.
6. **Barajas, D., Y. Jiang, and P. D. Nagy.** 2009. A unique role for the host ESCRT proteins in replication of Tomato bushy stunt virus. PLoS Pathog. **5:**e1000705.
7. **Buchkovich, N. J., Y. Yu, C. A. Zampieri, and J. C. Alwine.** 2008. The TORrid affairs of viruses: effects of mammalian DNA viruses on the PI3K-Akt-mTOR signalling pathway. Nat. Rev. Microbiol. **6:**266–275.
8. **Cid-Arregui, A., R. G. Parton, K. Simons, and C. G. Dotti.** 1995. Nocodazole-dependent transport, and brefeldin A-sensitive processing and sorting, of newly synthesized membrane proteins in cultured neurons. J. Neurosci. **15:**4259–4269.
9. **Cooray, S.** 2004. The pivotal role of phosphatidylinositol 3-kinase-Akt signal transduction in virus survival. J. Gen. Virol. **85:**1065–1076.
10. **Cui, Z. Q., Z. P. Zhang, X. E. Zhang, J. K. Wen, Y. F. Zhou, and W. H. Xie.** 2005. Visualizing the dynamic behavior of poliovirus plus-strand RNA in living host cells. Nucleic Acids Res. **33:**3245–3252.
11. **Denison, M. R.** 2008. Seeking membranes: positive-strand RNA virus replication complexes. PLoS Biol. **6:**e270.
12. **Egger, D., and K. Bienz.** 2005. Intracellular location and translocation of silent and active poliovirus replication complexes. J. Gen. Virol. **86:**707–718.
13. **Friedman, R. M., and I. K. Berezesky.** 1967. Cytoplasmic fractions associated with Semliki Forest virus ribonucleic acid replication. J. Virol. **1:**374–383.
14. **Friedman, R. M., J. G. Levin, P. M. Grimley, and I. K. Berezesky.** 1972. Membrane-associated replication complex in arbovirus infection. J. Virol. **10:**504–515.
15. **Froshauer, S., J. Kartenbeck, and A. Helenius.** 1988. Alphavirus RNA replicase is located on the cytoplasmic surface of endosomes and lysosomes. J. Cell Biol. **107:**2075–2086.
16. **Girao, H., M. I. Geli, and F. Z. Idrissi.** 2008. Actin in the endocytic pathway: from yeast to mammals. FEBS Lett. **582:**2112–2119.
17. **Gorchakov, R., N. Garmashova, E. Frolova, and I. Frolov.** 2008. Different types of nsP3-containing protein complexes in Sindbis virus-infected cells. J. Virol. **82:**10088–10101.
18. **Grimley, P. M., I. K. Berezesky, and R. M. Friedman.** 1968. Cytoplasmic structures associated with an arbovirus infection: loci of viral ribonucleic acid synthesis. J. Virol. **2:**1326–1338.
19. **Hagemeijer, M. C., M. H. Verheije, M. Ulasli, I. A. Shaltiel, L. A. de Vries, F. Reggiori, P. J. Rottier, and C. A. de Haan.** 2010. Dynamics of coronavirus replication-transcription complexes. J. Virol. **84:**2134–2149.
20. **Hawkins, P. T., K. E. Anderson, K. Davidson, and L. R. Stephens.** 2006. Signalling through Class I PI3Ks in mammalian cells. Biochem. Soc. Trans. **34:**647–662.
21. **Kääriäinen, L., and T. Ahola.** 2002. Functions of alphavirus nonstructural proteins in RNA replication. Prog. Nucleic Acid Res. Mol. Biol. **71:**187–222.
22. **Kaksonen, M., H. B. Peng, and H. Rauvala.** 2000. Association of cortactin with dynamic actin in lamellipodia and on endosomal vesicles. J. Cell Sci. **113:**4421–4426.
23. **Keränen, S., and L. Kääriäinen.** 1974. Isolation and basic characterization of temperature-sensitive mutants from Semliki Forest virus. Acta Pathol. Microbiol. Scand. B Microbiol. Immunol. **82:**810–820.
24. **Knight, Z. A., B. Gonzalez, M. E. Feldman, E. R. Zunder, D. D. Goldenberg, O. Williams, R. Loewith, D. Stokoe, A. Balla, B. Toth, T. Balla, W. A. Weiss, R. L. Williams, and K. M. Shokat.** 2006. A pharmacological map of the PI3-K family defines a role for p110α in insulin signaling. Cell **125:**733–747.
25. **Kopek, B. G., G. Perkins, D. J. Miller, M. H. Ellisman, and P. Ahlquist.** 2007. Three-dimensional analysis of a viral RNA replication complex reveals a virus-induced mini-organelle. PLoS Biol. **5:**e220.
26. **Kovács, M., J. Toth, C. Hetenyi, A. Malnasi-Csizmadia, and J. R. Sellers.** 2004. Mechanism of blebbistatin inhibition of myosin II. J. Biol. Chem. **279:**35557–35563.
27. **Kujala, P., T. Ahola, N. Ehsani, P. Auvinen, H. Vihinen, and L. Kääriäinen.** 1999. Intracellular distribution of rubella virus nonstructural protein P150. J. Virol. **73:**7805–7811.
28. **Kujala, P., A. Ikäheimonen, N. Ehsani, H. Vihinen, P. Auvinen, and L. Kääriäinen.** 2001. Biogenesis of the Semliki Forest virus RNA replication complex. J. Virol. **75:**3873–3884.
29. **Laakkonen, P., P. Auvinen, P. Kujala, and L. Kääriäinen.** 1998. Alphavirus

replicase protein NSP1 induces filopodia and rearrangement of actin filaments. J. Virol. **72:**10265–10269.
30. **Laakkonen, P., M. Hyvönen, J. Peränen, and L. Kääriäinen.** 1994. Expression of Semliki Forest virus Nsp1-specific methyltransferase in insect cells and in Escherichia coli. J. Virol. **68:**7418–7425.
31. **Lampio, A., I. Kilpelainen, S. Pesonen, K. Karhi, P. Auvinen, P. Somerharju, and L. Kääriäinen.** 2000. Membrane binding mechanism of an RNA virus-mapping enzyme. J. Biol. Chem. **275:**37853–37859.
32. **Liang, Z., and G. Li.** 2005. Recombinant Sindbis virus expressing functional GFP in the nonstructural protein nsP3. Gene Ther. Mol. Biol. **9:**317–324.
33. **Liljeström, P., and H. Garoff.** 1991. A new generation of animal cell expression vectors based on the Semliki Forest virus replicon. Biotechnology (NY) **9:**1356–1361.
34. **Lindmo, K., and H. Stenmark.** 2006. Regulation of membrane traffic by phosphoinositide 3-kinases. J. Cell Sci. **119:**605–614.
35. **Luzio, J. P., P. R. Pryor, and N. A. Bright.** 2007. Lysosomes: fusion and function. Nat. Rev. Mol. Cell Biol. **8:**622–632.
36. **Mackenzie, J.** 2005. Wrapping things up about virus RNA replication. Traffic **6:**967–977.
37. **Matteoni, R., and T. E. Kreis.** 1987. Translocation and clustering of endosomes and lysosomes depends on microtubules. J. Cell Biol. **105:**1253–1265.
38. **Mercer, J., and A. Helenius.** 2008. Vaccinia virus uses macropinocytosis and apoptotic mimicry to enter host cells. Science **320:**531–535.
39. **Mercer, J., and A. Helenius.** 2009. Virus entry by macropinocytosis. Nat. Cell Biol. **11:**510–520.
40. **Miller, S., and J. Krijnse-Locker.** 2008. Modification of intracellular membrane structures for virus replication. Nat. Rev. Microbiol. **6:**363–374.
41. **Mironov, A. A., G. V. Beznoussenko, A. Luini, and R. S. Polishchuk.** 2005. Visualizing intracellular events in vivo by combined video fluorescence and 3-D electron microscopy. Methods Enzymol. **404:**43–57.
42. **Mironov, A. A., R. S. Polishchuk, and G. V. Beznoussenko.** 2008. Combined video fluorescence and 3D electron microscopy. Methods Cell Biol. **88:**83–95.
43. **Novoa, R. R., G. Calderita, R. Arranz, J. Fontana, H. Granzow, and C. Risco.** 2005. Virus factories: associations of cell organelles for viral replication and morphogenesis. Biol. Cell **97:**147–172.
44. **Peränen, J., and L. Kääriäinen.** 1991. Biogenesis of type-I cytopathic vacuoles in Semliki Forest virus-infected BHK cells. J. Virol. **65:**1623–1627.
45. **Peränen, J., P. Laakkonen, M. Hyvönen, and L. Kääriäinen.** 1995. The alphavirus replicase protein Nsp1 is membrane-associated and has affinity to endocytic organelles. Virology **208:**610–620.
46. **Puhka, M., H. Vihinen, M. Joensuu, and E. Jokitalo.** 2007. Endoplasmic reticulum remains continuous and undergoes sheet-to-tubule transformation during cell division in mammalian cells. J. Cell Biol. **179:**895–909.
47. **Saeed, M. F., A. A. Kolokoltsov, A. N. Freiberg, M. R. Holbrook, and R. A. Davey.** 2008. Phosphoinositide-3 kinase-Akt pathway controls cellular entry of Ebola virus. PLoS Pathog. **4:**e1000141.
48. **Salonen, A., T. Ahola, and L. Kääriäinen.** 2005. Viral RNA replication in association with cellular membranes. Curr. Top. Microbiol. Immunol. **285:** 139–173.
49. **Salonen, A., L. Vasiljeva, A. Merits, J. Magden, E. Jokitalo, and L. Kääriäinen.** 2003. Properly folded nonstructural polyprotein directs the Semliki Forest virus replication complex to the endosomal compartment. J. Virol. **77:**1691–1702.
50. **Schuffenecker, I., I. Iteman, A. Michault, S. Murri, L. Frangeul, M. C. Vaney, R. Lavenir, N. Pardigon, J. M. Reynes, F. Pettinelli, L. Biscornet, L. Diancourt, S. Michel, S. Duquerroy, G. Guigon, M. P. Frenkiel, A. C. Brehin, N. Cubito, P. Despres, F. Kunst, F. A. Rey, H. Zeller, and S. Brisse.** 2006. Genome microevolution of Chikungunya viruses causing the Indian Ocean outbreak. PLoS Med. **3:**1058–1070.
51. **Schwartz, M., J. B. Chen, M. Janda, M. Sullivan, J. den Boon, and P. Ahlquist.** 2002. A positive-strand RNA virus replication complex parallels form and function of retrovirus capsids. Mol. Cell **9:**505–514.
52. **Smerdou, C., and P. Liljeström.** 1999. Two-helper RNA system for production of recombinant Semliki Forest virus particles. J. Virol. **73:**1092–1098.
53. **Soares, J. A., F. G. Leite, L. G. Andrade, A. A. Torres, L. P. De Sousa, L. S. Barcelos, M. M. Teixeira, P. C. Ferreira, E. G. Kroon, T. Souto-Padron, and C. A. Bonjardim.** 2009. Activation of the PI3K/Akt pathway early during vaccinia and cowpox virus infections is required for both host survival and viral replication. J. Virol. **83:**6883–6899.
54. **Soldati, T., and M. Schliwa.** 2006. Powering membrane traffic in endocytosis and recycling. Nat. Rev. Mol. Cell Biol. **7:**897–908.
55. **Spiro, D. J., W. Boll, T. Kirchhausen, and M. Wessling-Resnick.** 1996. Wortmannin alters the transferrin receptor endocytic pathway in vivo and in vitro. Mol. Biol. Cell **7:**355–367.
56. **Spuul, P., A. Salonen, A. Merits, E. Jokitalo, L. Kääriäinen, and T. Ahola.** 2007. Role of the amphipathic peptide of Semliki Forest virus replicase protein nsP1 in membrane association and virus replication. J. Virol. **81:**872–883.
57. **Straight, A. F., A. Cheung, J. Limouze, I. Chen, N. J. Westwood, J. R. Sellers, and T. J. Mitchison.** 2003. Dissecting temporal and spatial control of cytokinesis with a myosin II inhibitor. Science **299:**1743–1747.
58. **Swanson, J. A.** 2008. Shaping cups into phagosomes and macropinosomes. Nat. Rev. Mol. Cell Biol. **9:**639–649.
59. **Vonderheit, A., and A. Helenius.** 2005. Rab7 associates with early endosomes to mediate sorting and transport of Semliki Forest virus to late endosomes. PLoS Biol. **3:**e233.
60. **Wang, R. Y. L., and P. D. Nagy.** 2008. Tomato bushy stunt virus co-opts the RNA-binding function of a host metabolic enzyme for viral genomic RNA synthesis. Cell Host Microbe **3:**178–187.
61. **Weber, F., V. Wagner, S. B. Rasmussen, R. Hartmann, and S. R. Paludan.** 2006. Double-stranded RNA is produced by positive-strand RNA viruses and DNA viruses but not in detectable amounts by negative-strand RNA viruses. J. Virol. **80:**5059–5064.
62. **Welsch, S., S. Miller, I. Romero-Brey, A. Merz, C. K. Bleck, P. Walther, S. D. Fuller, C. Antony, J. Krijnse-Locker, and R. Bartenschlager.** 2009. Composition and three-dimensional architecture of the dengue virus replication and assembly sites. Cell Host Microbe **5:**365–375.
63. **Wölk, B., B. Büchele, D. Moradpour, and C. M. Rice.** 2008. A dynamic view of hepatitis C virus replication complexes. J. Virol. **82:**10519–10531.